UC San Diego
UC San Diego Previously Published Works

Title

Ultrashort Echo Time (UTE) MRI porosity index (PI) and suppression ratio (SR) correlate with the cortical bone microstructural and mechanical properties: Ex vivo study

Permalink

Authors

Jerban, Saeed

Ma, Yajun

Alenezi, Salem

et al.

Peer reviewed

Ultrashort Echo Time (UTE) MRI porosity index (PI) and suppression ratio (SR) correlate with the cortical bone microstructural and mechanical properties: Ex vivo study

Saeed Jerban[1,2,3,*], **Yajun Ma**[1,2], **Salem Alenezi**[4], **Dina Moazamian**[1], **Jiyo Athertya**[1], **Hyungseok Jang**[1,2], **Erik Dorthe**[5], **Darryl Dlima**[5], **Gina Woods**[6], **Christine B. Chung**[1,2], **Eric Y. Chang**[1,2], **Jiang Du**[1,2,*]

[1]Department of Radiology, University of California, San Diego, La Jolla, CA, USA

[2]Radiology Service, Veterans Affairs San Diego Healthcare System, San Diego, La Jolla, CA, USA

[3]Department of Orthopedic Surgery, University of California, San Diego, La Jolla, CA, USA

[4]Research and Laboratories Sector, Saudi Food and Drug Authority, Riyadh, KSA

[5]Shiley Center for Orthopedic Research and Education at Scripps Clinic, La Jolla, CA, USA

[6]Department of Medicine, University of California, San Diego, La Jolla, CA, USA

Abstract

Ultrashort echo time (UTE) MRI can image and consequently enable quantitative assessment of cortical bone. UTE-MRI-based evaluation of bone is largely underutilized due to the high cost and time demands of MRI in general. The signal ratio in dual-echo UTE imaging, known as porosity index (PI), as well as the signal ratio between UTE and inversion recovery UTE (IR-UTE) imaging, known as the suppression ratio (SR), are two rapid UTE-based bone evaluation techniques (~ 5 mins scan time each), which can potentially reduce the time demand and cost in future clinical studies. This study aimed to investigate the correlations of PI and SR measures with cortical bone microstructural and mechanical properties. Cortical bone strips (n=135) from tibial and femoral midshafts of 37 donors (61±24 years old) were scanned using a dual-echo 3D Cones UTE sequence and a 3D Cones IR-UTE sequence for PI and SR calculations, respectively. Average bone mineral density, porosity, and pore size were measured using microcomputed tomography (μCT). Bone mechanical properties were measured using 4-point bending tests. The μCT measures showed significant correlations with PI (moderate to strong, R=0.68-0.71) and SR (moderate, R=0.58-0.68). Young's modulus, yield stress, and ultimate stress demonstrated significant moderate correlations with PI and SR (R=0.52-0.62) while significant strong correlations with μCT measures (R>0.7). PI and SR can potentially serve as fast

[*]**Corresponding authors:** • **Jiang Du,** Department of Radiology, University of California, San Diego, 9500 Gilman Dr., La Jolla, CA 92093, USA, jiangdu@health.ucsd.edu , Phone: +1 858 246 2248, Fax: +1 888 960 5922; • **Saeed Jerban**, Department of Radiology, University of California, San Diego, 9500 Gilman Dr., La Jolla, CA 92093, USA, sjerban@health.ucsd.edu Phone: +1 858 246 2248, Fax: +1 888 960 5922.

and noninvasive (non-ionizing radiation) biomarkers for evaluating cortical bone in various bone diseases.

Keywords

cortical bone; MRI; ultrashort echo time; porosity index; suppression ratio; bone mechanics

1. INTRODUCTION

Magnetic resonance imaging (MRI) has been increasingly used for cortical bone assessment [1–9], first to avoid exposure to ionizing radiation associated with x-ray-based techniques [5,10–12] and second to provide an opportunity for simultaneous evaluation of the surrounding soft tissues [13]. Notably, clinical MRI is not able to detect a considerable signal from cortical bone due to its ultrashort apparent transverse relaxation time (T2*). However, ultrashort echo time (UTE) MRI can image cortical bone, consequently enabling quantitative assessment of cortical bone [5–8,10,14–19]. Typically, UTE-MRI techniques can acquire the bone signal in less than fifty microseconds after radiofrequency (RF) excitation and before a significant decay in transverse magnetization.

UTE-MRI-based evaluation of bone is underutilized partly due to the high cost and time demands of MRI in general. For these reasons, different research groups have focused on developing rapid and efficient UTE-MRI-based methods to facilitate clinical translational imaging of bone. The signal ratio calculation in dual-echo UTE imaging [20] and the signal ratio between UTE and inversion recovery UTE (IR-UTE) [21] are two remarkable examples of rapid UTE-based bone evaluation techniques, each of which takes less than 5 minutes. It should be noted that the required time for PI and SR measures depends on the UTE acquisition techniques, which can be two-dimensional (2D) (using cartesian or radial trajectories) [22,23] or three-dimensional (3D) (using cartesian, radial, spiral, or cones trajectories) [9]. In general, a 2D UTE sequence is faster than a 3D UTE sequence, and a spiral acquisition is faster than a radial or cartesian acquisition.

Cortical bone is mainly comprised of a mineral matrix (~40% by volume), organic matrix (~30%), and water (~20%) [24,25]. In healthy bone, most of the water is bound to the organic and mineral matrices which is called "bound water" (BW) [5,26–31]. A smaller portion of bone water called "pore water" (PW) resides in different pores such as Haversian canals (10-200 μm), lacunae (1-10 μm), and canaliculi (0.1-1 μm) [24,26]. The T2* of PW is typically above 2 ms which is significantly higher than the T2* of BW which is around 0.3 ms [8,32–34]. Therefore, it can be hypothesized that there is no contribution from BW protons in any acquired MRI signal at TEs above 2 ms (the signal is mainly from PW and fat residing in the macroscopic pores of cortical bone). Based upon this assumption, Rajapakse et al. [20] proposed a dual-echo UTE imaging technique to calculate the so-called porosity index (PI), which is the signal ratio between two MRI images, one with UTE (TE < 0.05ms) and one with TE = 2.2 ms (where bound water signal has decayed to near zero, and pore water and fat signals are in-phase at 3T). The first echo image represents the total detectable signal from bone, including BW, PW, and fat. The second echo represents

mostly PW and fat signals (no BW signal). Therefore, the signal ratio between the two images is hypothesized to correlate with the pores' volume (filled with PW and/or fat) to the total volume. Although this technique does not estimate the absolute PW content or fat content, it gives an estimation of bone porosity. In previous validation studies, PI in a limited number of human cadaveric tibiae has shown significant correlations with μCT-based porosity (n=16), donor age (n=16), mechanical compression stiffness performed on whole-cross-section tibial specimens (n=18), and collagen estimation from near-infrared spectroscopy (n=18) [20,35].

Li et al. have proposed another UTE-based rapid technique for cortical bone evaluation, called the suppression ratio (SR), defined as the ratio between the bone UTE signal and the UTE signal after long-T2 suppression performed via dual-band saturation-prepared UTE (DB-UTE) or IR-UTE [21]. As mentioned before, the UTE image represents the total detectable signal from bone, including BW, PW, and fat, while the IR-UTE image represents only the BW signal. Therefore, a higher SR value means higher PW and fat signals, which imply a higher porosity value. In previous ex vivo validation studies of a limited number of specimens (n=13), SR demonstrated significant correlations with μCT-based bone porosity and donor age [21]. SR performed in vivo demonstrated significant correlations with volumetric bone mineral density and participants' age [21].

The goal of this study was to investigate the correlations of PI and SR measures of 135 cadaveric human cortical bone specimens with the microstructural and tensile mechanical properties obtained from four-point bending tests. This study examines the performance of such rapid UTE-based techniques beyond the feasibility studies performed by the original developers.

2. MATERIALS AND METHODS

2.1. Sample preparation

One hundred thirty-five cortical bone specimens were harvested from the tibial and femoral midshafts of 37 donors (61±24 years old) provided by a non-profit whole-body donation company (United Tissue Network, Phoenix, AZ). The middle parts of the tibial and femoral shafts were cut into 40 mm segments using a commercial band saw. One to three rectangular bone strips were excised from each segment using a low-speed diamond saw (Isomet 1000, Buehler, IL). The final dimensions of the rectangular bone strips were approximately 4mm×2mm×40mm. Bone strips were kept frozen on average for two weeks before MRI scans. After being thawed, bone strips were immersed in phosphate-buffered saline (PBS) for four hours at room temperature before the MRI scans to compensate for potential dehydration occurred throughout the specimen preparation. Finally, strips were randomly distributed into eight groups and placed in 30-mL syringes (15-20 strips per syringe) filled with perfluoropolyether (Fomblin, Ausimont, Thorofare, NJ) to minimize dehydration and susceptibility artifacts.

2.2.   UTE-MRI protocol

The UTE-MRI scans were performed on a 3T clinical scanner (GE Healthcare, Waukesha, WI) using a homemade 1-inch diameter transmit/receive birdcage coil. The UTE-MRI scans involved a) the dual-echo 3D Cones UTE sequence (repetition time (TR) = 100 ms, TE = 0.032 and 2.2 ms, flip angle (FA) = 10°) for PI measurement (Eq. 1) [20] and, b) the 3D Cones IR-UTE sequence (TR = 100 ms, TI = 45 ms, and TE = 0.032 ms, FA = 20°) for SR calculation (Eq. 2) [21]. The adiabatic inversion pulse used in this study was centered at −220 Hz from the water peak. The IR pulse with a spectral bandwidth of 1150 Hz provides robust coverage of fat and pore water peaks. The IR pulse duration was 8.6 ms. Other imaging parameters included: field of view (FOV) = 40 mm, matrix size = 160×160, in-plane pixel size = 0.25 mm, slice thickness = 2 mm, receiver bandwidth = 125 kHz, and total scan time ≈ 10 mins.

$$PI = \frac{2nd\ Echo\ Signal\ (TE = 2.2\ ms)}{UTE\ signal\ (TE = 0.032\ ms)} \qquad \text{Eq. 1}$$

$$SR = \frac{UTE\ signal\ (TE = 0.032\ ms)}{IR\ UTE\ signal\ (TE = 0.032\ ms)} \qquad (2)$$

2.3.   Micro-computed tomography (μCT)

Bone strips inside the 30-mL syringes were scanned using a Skyscan 1076 (Kontich, Belgium) μCT scanner at 9 μm isotropic voxel size. For measuring BMD in addition to bone porosity, specimens were scanned in the presence of two hydroxyapatite phantoms (0.25 and 0.5 gr/cm^3). Other scanning parameters were as follows: a 0.05 mm aluminum filter in addition to a 0.038 mm copper filter, 100 kV, 100 mA, 0.3° rotation step, and five frame-averaging. The total μCT scan time was twelve hours for all bone strips.

The μCT image segmentation was performed by gray level thresholding. The gray level threshold was selected for each set of μCT data using the gray level histograms and visual investigation of the bone-pore interface in raw μCT images. Microstructural properties of each bone strip were calculated in a stack of 200 μCT slices in the middle of the bone strips, which corresponded to the 2 mm slice of MRI images. Bone porosity was estimated as the ratio of the number of voxels in pores to the total number of voxels included in each bone strip. Pore size was also calculated as the diameter of the largest covering sphere. Local BMD at each voxel was calculated using a linear function of the voxel's gray level, which is determined based on the obtained gray levels of the two known BMD phantoms. Average pore size and BMD were calculated for each bone strip over the abovementioned 200 μCT slices.

2.4.   Mechanical properties measurement

The tensile mechanical properties of each bone strip were measured using a four-point bending setup [36]. It is assumed that the tensile side of a bone strip (brittle material) fails under bending because of lower tensile properties compared with compressive properties

in such materials. The actual assembled four-point bending setup is illustrated in Figure 1A. The setup was comprised of four tungsten carbide pins (3-mm diameter) mounted on two aluminum holders. The upper holder was connected to the hydraulic actuator of a mechanical testing machine (model 8511.20, Instron, Norwood, MA, USA). The lower aluminum holder was connected to a 4500 N load cell (Sensotec 1000 LBS). Each bone strip was positioned on the lower pins. The contact between loading pins and the bone strip was achieved by manually lowering the actuator. The mechanical failure test was performed in the displacement-controlled mode for 30 to 60 seconds at 0.1 mm/s until specimen fracture while the applied force was continuously recorded.

Stress-strain (σ-ε) relation curve on the beam's surface, which experiences the highest mechanical stress in bending between loading pins (middle of the beam length) was determined from the measured force and displacement data, as well as from the accurate μCT-based bone strip dimensions. As described in more detail in previous studies [33,37], ASTM C1674 protocol (for specimens with relatively large pores, pore/thickness >15) [38], and a Weibull modulus [39,40] of four were considered to correct the estimated stresses. Modified stresses were used in determining the stress-strain curves (Figure 1B). Young's modulus of elasticity (E) was determined from the linear section of the stress-strain curve. A yield point was defined at a point on the curve where the curve deviated by a strain of 0.002 from the linear part of the curve described by Young's modulus [36]. The yield point was used to determine both yield stress (σ_Y) and yield strain (ε_Y). The maximum stress and its corresponding strain were assigned to the ultimate stress (σ_U) and ultimate strain (ε_U), respectively. The failure energy or work to failure (W_F) was defined as the area below the stress-strain curve.

2.5. Statistical analyses

Normal distribution of PI and SR values, porosity, pore size, and mechanical variables were examined using the Kolmogorov-Smirnov test. Spearman's rank correlations were calculated between the rapid UTE-MRI indices (PI and SR), microstructural parameters (porosity and pore size), and mechanical properties (Young's modulus, yield stress, ultimate stress, and failure energy), assuming all specimens were considered to be independent of each other. Spearman's correlations were repeated using one averaged sample per donor to avoid the potential impact of the specimens' interdependencies on the statistical analysis. The number of specimens per donor was not constant (1-4 samples per donor) and the harvesting location was not consistent for all specimens (e.g., anterior or posterior side of femur and tibia), therefore the averaged measures per donor were used instead of a randomly selected sample per donor. Correlations with P-values below 0.05 were considered significant. All measurements and models were performed using MATLAB (version 2017, The Mathworks Inc., Natick, MA, USA) codes developed in-house.

3. RESULTS

Figure 2A shows the UTE-MRI image (TE = 0.032 ms) of twenty bone strips in a 30-ml syringe scanned in the axial plane, showing the 4mm x 2mm cross section of samples. Figure 2B and 2C show the 2nd echo MRI image at TE = 2.2 ms and IR-UTE image,

respectively, for the same specimens. The μCT images of two representative cortical bone strips with different porosities are shown in Figure 2D, with 15% and 33% average porosities, respectively. Specimens I and II, indicated with yellow dashed-line boxes in Figure 2A, were harvested from a 47-year-old male and a 57-year-old female, respectively. Specimen II obviously shows higher signal in UTE and 2nd TE images.

Figure 3A and 3B illustrate the PI and SR pixel maps, respectively, for the bone specimens shown in Figure 2. Between the two representative samples highlighted in Figure 2, specimen II demonstrates higher PI and SR values compared with specimen I.

The average, standard deviation (SD), and ranges of MRI, μCT, and mechanical properties of bone strips are presented in Table 1.

Spearman's correlations between MRI-based measures (PI and SR) and microstructural and mechanical properties are presented in Table 2, assuming all specimens were considered to be independent of each other (n=135). The μCT measures showed significant correlations with PI (moderate to strong, R=0.68-0.71) and SR (moderate, R=0.58-0.68). Young's modulus, yield stress, and ultimate stress demonstrated significant moderate correlations with PI and SR (R=0.52-0.62) while significant strong correlations with μCT measures (R>0.7). PI correlates higher than SR with microstructural and mechanical properties. PI and SR were significantly correlated.

Spearman's correlations between MRI-based measures and microstructural and mechanical properties are presented in the supplemental Table 1S when one averaged sample per donor was included in the statistical analysis. A similar range of correlations with slight differences was obtained by including only one averaged sample. Specifically, the correlations between MRI and μCT measures increased slightly by including one sample per donor while correlations with mechanical properties decreased slightly.

Figures 4 demonstrates the scatter plots and the linear trendlines of PI and SR versus μCT-based BMD, porosity, and pore size. As expected, the higher the PI and SR, the higher the porosity and pore size.

Figures 5 illustrates the scatter plots and the linear trendlines of PI and SR versus Young's modulus, yield stress, ultimate stress, and failure energy, respectively. As expected, bone mechanical properties were lower for specimens with higher PI and SR.

4. DISCUSSION

This study examined the correlations of two reported rapid UTE-MRI-based indices, PI and SR, with microstructural and mechanical properties of human cortical bone strips. Rapid UTE-MRI-based techniques for bone assessment, such as PI and SR, can be considered *in vivo*-translatable techniques due to their simplicity, time efficiency, and, importantly, their noninvasive and ionizing-radiation-free nature.

This investigation was performed on a considerably large number of bone specimens (n = 135 from 37 donors) compared with the previous feasibility and validation studies (n<18)

[20,21,35]. Since an ideal bone assessment technique is expected to be able to detect intra- and inter-patient differences, using a few specimens per donor in this study is considered reasonable. However, the calculated correlation coefficients and their statistical significance might be affected by the interdependencies between specimens. It should be noted that a similar range of correlations was obtained when only one averaged sample per donor was included in the statistical analysis of this study (n=135 in Table 2, n=37 in Table 1S).

The previously reported correlations of PI and SR with μCT-based structural parameters (R≈0.9 [20,21]) were much higher than the values demonstrated in this study. Such differences might be due to variations in the number and type of specimens (tibial shaft cross-section versus cortical bone strips), the MRI and μCT scanners, the employed coils, scanning protocols, and especially the performance of the IR-UTE pulse sequence. The IR-UTE imaging protocol with a shorter TR/TI combination in this study is likely to provide more efficient suppression of pore water and, thus, more selective imaging of bound water in cortical bone than prior approaches in which significantly longer TRs and TIs were used [20,41].

Tensile mechanical properties in uniform beams under bending conditions were investigated in this study. Mechanical compression tests were previously performed on whole-cross-section tibial specimens in order to investigate the correlation between PI and mechanical properties [35]. However, obtained mechanical properties in such compression tests are not only related to the average bone quality but also the cross-sectional area and shape of the tibial shaft. Moreover, it is challenging to assume uniform mechanical properties for whole-cross-section tibial specimens. In the current study, bone strips with known cross-sections undergoing four-point mechanical bending tests were used to avoid the bone cross-section influence on the results. This study was the first to investigate the SR correlations with mechanical properties. Young's modulus, yield stress, and ultimate stress demonstrated significant moderate correlations with PI and SR. In comparison to SR, PI showed higher correlations with microstructural and mechanical properties.

In addition to PI and SR, other UTE-MRI-based methods have been investigated in the literature for their correlations with cortical bone mechanical properties [6–8]. Remarkably, the correlation coefficients between mechanical properties and other more sophisticated UTE-based techniques have been in the range of correlation coefficients achieved by the rapid UTE-MRI-based indices (PI and SR). Fernandez et al. [42] found negative correlations between bone mechanical properties and total water content in whole cross-sections of long bones measured by NMR spectroscopy at 9.4T magnetic field (n=11, R=0.72-0.77). Horch et al. and Nyman et al. [27,43] demonstrated significant positive correlations between estimated BW pool from NMR spectroscopy at 4.7T magnetic field and cortical bone mechanical properties in bone strips (n=18, R=0.60, and n=40, R=0.82). They also showed significant negative correlations between PW pool and mechanical properties (n=18, R=0.45, and n=40, R=0.78). Later, Horch et al. [3] used UTE-MRI at 4.7T magnetic field for direct imaging of BW and PW and reported significant correlations with mechanical properties of bone strips (n=14, R=0.68-0.83). Granke et al. [44] investigated the correlations between bone NMR spectroscopy results of PW and BW peaks at 4.7T magnetic field with human bone fracture toughness. They found significant correlations

between NMR-derived BW fraction and fracture toughness properties of cortical bone strips (n=62, R=0.63). Bae et al. [45] presented significant correlations between bicomponent T2* fitting results performed at 3T magnetic field and the mechanical properties of human cortical bone strips (n=44, R=0.54). Later, Manhard et al. [46] studied the correlations between direct imaging of PW and BW contents at 3T with bone fracture toughness in whole cross-sections of long cortical bone. They found that BW content significantly correlated with toughness, defined as the energy dissipated during fracture (n=20, R=0.51). Chang et al. [47] found significant correlations between bone mechanical properties and magnetization transfer ratio (MTR) between collagen and water pools at 3T (n=122, R=0.55). Jerban et al. employed a UTE-based two-pool MT modeling to measure collagen proton fraction at 3T and observed significant correlations with bone strips' mechanical properties (n=156, R=0.60-0.61) [48]. Recently, Jerban et al. used tricomponent T2* fitting results performed at 3T to consider the fat content in cortical bone, which showed significant correlations with mechanical properties of human cortical bone strips (n=135, R=0.58-0.62) [33].

It should be noted that the required scan time for all mentioned UTE MRI techniques can be improved by different acceleration techniques such as spokes stretching in Cones [49], compressed sensing [50,51], and parallel imaging [52,53]. Since both PI and SR measurements require only two acquisitions, they may be faster than other techniques which require multiple acquisitions [30,32–34,37,53–58] if similar acceleration techniques are utilized. This applies to other rapid techniques that use only two acquisitions, such as the PW and BW direct imaging techniques, employed by Horch et al. [3] and Manhard et al. [46], as well as the MTR technique employed by Chang et al. [47].

This study had a number of limitations. First, this study was performed *ex vivo* on bone specimens cut from pure cortical bone layers, with bone marrow and surrounding muscles removed with a scalpel. The presence of fat, muscles and other soft tissues, lower spatial resolution, a higher body temperature [19], and subject motion will all contribute to the reduced performance of all UTE-MRI-based imaging techniques *in vivo* compared with *ex vivo* studies. Second, PI correlation coefficients with microstructural and mechanical parameters were higher than those of SR. The calculated value for SR is related to the selection of TR and TI, which was based on our experience with SNR improvement and efficient PW signal nulling. Theoretically, each TR/TI combination can only null long-T2 species with a single T1, especially when the TR is long. Our past simulation and experimental studies [54,55] suggest that a shorter TR/TI combination provides more efficient long-T2 signal suppression than a longer TR/TI combination in IR-UTE imaging. The shorter TR/TI combination improves the suppression of long-T2 species with a broad range of T1s. This is especially important in selective imaging of BW in cortical bone, where PW may have a broad range of T1s due to the surface relaxation mechanism (i.e., water in smaller pores and that closer to pore surfaces may have higher T1 relaxation rates) [56]. On the other hand, using a shorter TR results in a lower SNR in the IR-UTE images which may affect the quantitative measures. Therefore, a systematic comparison between various TRs, TR/TI combinations, and FAs in IR-UTE remains to be investigated for selective imaging of bound water in cortical bone. Moreover, comparisons with dual-adiabatic IR pulses (invert and null signals from fat and PW separately) [57–60] can help

optimize the SR measurement. Third, the IR-UTE data acquisition can be affected by the B1 inhomogeneity over the investigated specimens within the employed coil. Supplemental Figure 1S shows the measured B1 map for one set of specimens in this study. Although the B1 field was reasonably homogenous for most of the investigated specimens, some inhomogeneities were seen near the lower and upper edges of the syringe. This B1 variation was relatively small (<10%) and should not affect the long-T2 inversion efficiency as the IR-UTE sequence used adiabatic inversion pulses, which are known to provide uniform inversion even with a relatively inhomogeneous B1 field [61]. However, this B1 variation is expected to affect the actual imaging flip angle, leading to minor errors in PI and SR measurements as the numerator and denominator in Eq.1 are affected similarly. Fourth, despite the efforts to keep bone specimens wet, some degree of bone dehydration was expected during the sample preparation steps. Although PBS may be different from the actual intraosseous liquid in bone, soaking the specimens in PBS would presumably compensate for the potential hydration with negligible impacts on the MRI properties. However, its impact on the four-point mechanical test results needs more investigation. Fifth, accurate medical records of the donors were not available to be considered in the exclusion criteria. Some diseases such as diabetes are suspected to impact cortical bone mechanical properties independently from their porosity [62–65], thus including such donors in this study might affect the investigated correlations.

5. Conclusion

The correlations of two recently developed rapid UTE-MRI-based indices, PI and SR, were investigated with microstructural and mechanical properties of human cortical bone strips. PI and SR can be considered noninvasive, ionizing-radiation-free, and *clinically* translatable due to their simplicity and time efficiency. PI and SR showed significant correlations with microstructural (BMD, porosity, and pore size) and mechanical properties (Young's modulus, yield stress, and ultimate stress) of cortical bone specimens. PI correlated better than SR with the microstructural and mechanical properties of bone strips. This study highlighted PI and SR, as potential rapid techniques to assess cortical bone mechanical properties and intracortical bone microstructure.

Supplementary Material

Refer to Web version on PubMed Central for supplementary material.

Acknowledgements

Abbreviations:

MR	magnetic resonance
MRI	magnetic resonance imaging

3D	three-dimensional
3D-UTE	three-dimensional ultrashort echo time imaging
RF	radio frequency
FOV	field of view
ROI	region of interest
TE	echo time
TR	repetition time
CT	computed tomography
μCT	micro-computed tomography
FA	flip angle
BMD	bone mineral density
PBS	phosphate-buffered saline
PI	porosity index
SR	suppression ratio

8. References

[1]. Reichert ILH, Robson MD, Gatehouse PD, He T, Chappell KE, Holmes J, Girgis S, Bydder GM, Magnetic resonance imaging of cortical bone with ultrashort TE pulse sequences, Magn Reson Imaging. 23 (2005) 611–618. 10.1016/j.mri.2005.02.017. [PubMed: 16051035]

[2]. Techawiboonwong A, Song HK, Wehrli FW, In vivo MRI of submillisecond T2 species with two-dimensional and three-dimensional radial sequences and applications to the measurement of cortical bone water, NMR Biomed. (2008). 10.1002/nbm.1179.

[3]. Horch RA, Gochberg DF, Nyman JS, Does MD, Clinically compatible MRI strategies for discriminating bound and pore water in cortical bone, Magn Reson Med. 68 (2012) 1774–1784. 10.1002/mrm.24186. [PubMed: 22294340]

[4]. Du J, Carl M, Bydder M, Takahashi A, Chung CB, Bydder GM, Qualitative and quantitative ultrashort echo time (UTE) imaging of cortical bone, Journal of Magnetic Resonance. 207 (2010) 304–311. 10.1016/j.jmr.2010.09.013. [PubMed: 20980179]

[5]. Du J, Bydder GM, Qualitative and quantitative ultrashort-TE MRI of cortical bone, NMR Biomed. 26 (2013) 489–506. 10.1002/nbm.2906. [PubMed: 23280581]

[6]. Jerban S, Chang DG, Ma Y, Jang H, Chang EY, Du J, An Update in Qualitative Imaging of Bone Using Ultrashort Echo Time Magnetic Resonance, Front Endocrinol (Lausanne). 11 (2020) 677–689. 10.3389/fendo.2020.555756.

[7]. Ma Y-J, Jerban S, Jang H, Chang D, Chang EY, Du J, Quantitative Ultrashort Echo Time (UTE) Magnetic Resonance Imaging of Bone: An Update, Front Endocrinol (Lausanne). 11 (2020) 667–676. 10.3389/fendo.2020.567417.

[8]. Jerban S, Ma Y, Wei Z, Jang H, Chang EY, Du J, Quantitative Magnetic Resonance Imaging of Cortical and Trabecular Bone, Semin Musculoskelet Radiol. 24 (2020) 386–401. 10.1055/s-0040-1710355. [PubMed: 32992367]

[9]. Masoud Afsahi A, Ma Y, Jang H, Jerban S, Chung CB, Chang EY, Du J, Ultrashort Echo Time Magnetic Resonance Imaging Techniques: Met and Unmet Needs in Musculoskeletal Imaging, (2021). 10.1002/jmri.28032.

[10]. Chang EY, Du J, Chung CB, UTE imaging in the musculoskeletal system, Journal of Magnetic Resonance Imaging. 41 (2015) 870–883. 10.1002/jmri.24713. [PubMed: 25045018]

[11]. Manhard MK, Nyman JS, Does MD, Advances in imaging approaches to fracture risk evaluation, Translational Research. 181 (2017) 1–14. 10.1016/j.trsl.2016.09.006. [PubMed: 27816505]

[12]. Wehrli FW, Magnetic resonance of calcified tissues, Journal of Magnetic Resonance. 229 (2013) 35–48. 10.1016/j.jmr.2012.12.011. [PubMed: 23414678]

[13]. Jerban S, Ma Y, Namiranian B, Ashir A, Shirazian H, Zhao W, Wu M, Cai Z, Le N, Du J, Chang EYEY, Wei Z, Le N, Wu M, Cai Z, Du J, Chang EYEY, Age-related decrease in collagen proton fraction in tibial tendons estimated by magnetization transfer modeling of ultrashort echo time magnetic resonance imaging (UTE-MRI), Sci Rep. November (2019) 17974. 10.1038/s41598-019-54559-3. [PubMed: 31784631]

[14]. Jerban S, Ma Y, Wong JH, Nazaran A, Searleman A, Wan L, Williams J, Du J, Chang EY, Ultrashort echo time magnetic resonance imaging (UTE-MRI) of cortical bone correlates well with histomorphometric assessment of bone microstructure, Bone. 123 (2019) 8–17. 10.1016/j.bone.2019.03.013. [PubMed: 30877070]

[15]. Zhao X, Song HK, Seifert AC, Li C, Wehrli FW, Feasibility of assessing bone matrix and mineral properties in vivo by combined solidstate 1H and 31P MRI, PLoS One. 12 (2017) 1–16. 10.1371/journal.pone.0173995.

[16]. Lu X, Jerban S, Wan L, Ma Y, Jang H, Le N, Yang W, Chang EY, Du J, Three Dimensional Ultrashort Echo Time Imaging with Tri-component Analysis for Human Cortical Bone, Magn Reson Med. 82 (2019) 348–355. 10.1002/mrm.27718. [PubMed: 30847989]

[17]. Jerban S, Lu X, Jang H, Ma Y, Namiranian B, Le N, Li Y, Chang EY, Du J, Significant correlations between human cortical bone mineral density and quantitative susceptibility mapping (QSM) obtained with 3D Cones ultrashort echo time magnetic resonance imaging (UTE-MRI), Magn Reson Imaging. 62 (2019) 104–110. 10.1016/j.mri.2019.06.016. [PubMed: 31247253]

[18]. Jerban S, Ma Y, Li L, Jang H, Wan L, Guo T, Searleman A, Chang EY, Du I, Du J, Volumetric Mapping of Bound and Pore Water as well as Collagen Protons in Cortical Bone Using 3D Ultrashort Echo Time Cones MR Imaging Techniques, Bone. 127 (2019) 120–128. 10.1016/j.bone.2019.05.038. [PubMed: 31176044]

[19]. Jerban S, Szeverenyi N, Ma Y, Guo T, Namiranian B, To S, Jang H, Eric Y. Chang, Du J, Ultrashort echo time MRI (UTE-MRI) quantifications of cortical bone varied significantly at body temperature compared with room temperature, Investig Magn Reson Imaging. 23 (2019) 00. 10.13104/imri.2019.23.3.000.

[20]. Rajapakse CS, Bashoor-Zadeh M, Li C, Sun W, Wright AC, Wehrli FW, Volumetric Cortical Bone Porosity Assessment with MR Imaging: Validation and Clinical Feasibility., Radiology. 276 (2015) 526–35. 10.1148/radiol.15141850. [PubMed: 26203710]

[21]. Li C, Seifert AC, Rad HS, a Bhagat Y, Rajapakse CS, Sun W, Lam SCB, Wehrli FW, Cortical Bone Water Concentration: Dependence of MR Imaging Measures on Age and Pore Volume Fraction., Radiology. 272 (2014) 796–806. 10.1148/radiol.14132585. [PubMed: 24814179]

[22]. Manhard MK, Harkins KD, Gochberg DF, Nyman JS, Does MD, 30-Second bound and pore water concentration mapping of cortical bone using 2D UTE with optimized half-pulses, Magn Reson Med. 77 (2017) 945–950. 10.1002/mrm.26605. [PubMed: 28090655]

[23]. Harkins KD, Ketsiri T, Nyman JS, Does MD, Fast bound and pore water mapping of cortical bone with arbitrary slice oriented two-dimensional ultra-short echo time, Magn Reson Med. 89 (2023) 767–773. 10.1002/mrm.29484. [PubMed: 36226656]

[24]. Cowin SC, Bone poroelasticity, J Biomech. 32 (1999) 217–238. 10.1016/S0021-9290(98)00161-4. [PubMed: 10093022]

[25]. Wehrli FW, Song HK, Saha PK, Wright AC, Quantitative MRI for the assessment of bone structure and function, NMR Biomed. 19 (2006) 731–764. 10.1002/nbm. [PubMed: 17075953]

[26]. Wang X, Ni Q, Determination of cortical bone porosity and pore size distribution using a low field pulsed NMR approach, Journal of Orthopaedic Research. 21 (2003) 312–319. 10.1016/S0736-0266(02)00157-2. [PubMed: 12568964]

[27]. Nyman JS, Ni Q, Nicolella DP, Wang X, Measurements of mobile and bound water by nuclear magnetic resonance correlate with mechanical properties of bone, Bone. 42 (2008) 193–199. 10.1016/j.bone.2007.09.049. [PubMed: 17964874]

[28]. Horch RA, Nyman JS, Gochberg DF, Dortch RD, Does MD, Characterization of 1H NMR signal in human cortical bone for magnetic resonance imaging., Magnetic Resonance in Medicine : Official Journal of the Society of Magnetic Resonance in Medicine / Society of Magnetic Resonance in Medicine. 64 (2010) 680–687. 10.1002/mrm.22459.

[29]. Diaz E, Chung CB, Bae WC, Statum S, Znamirowski R, Bydder GM, Du J, Ultrashort echo time spectroscopic imaging (UTESI): an efficient method for quantifying bound and free water, NMR Biomed. 25 (2012) 161–168. 10.1002/nbm.1728. [PubMed: 21766381]

[30]. Biswas R, Bae WC, Diaz E, Masuda K, Chung CB, Bydder GM, Du J, Ultrashort echo time (UTE) imaging with bi-component analysis: Bound and free water evaluation of bovine cortical bone subject to sequential drying, Bone. 50 (2012) 749–755. 10.1016/j.bone.2011.11.029. [PubMed: 22178540]

[31]. Ong HH, Wright AC, Wehrli FW, Deuterium nuclear magnetic resonance unambiguously quantifies pore and collagen-bound water in cortical bone, Journal of Bone and Mineral Research. 27 (2012) 2573–2581. 10.1002/jbmr.1709. [PubMed: 22807107]

[32]. Jerban S, Ma Y, Wong JHJHJH, Nazaran A, Searleman A, Wan L, Williams J, Du J, Chang EYEY, Ultrashort echo time magnetic resonance imaging (UTE-MRI) of cortical bone correlates well with histomorphometric assessment of bone microstructure, Bone. 123 (2019) 8–17. 10.1016/j.bone.2019.03.013. [PubMed: 30877070]

[33]. Jerban S, Lu X, Dorthe EW, Alenezi S, Ma Y, Kakos L, Jang H, Sah RL, Chang EY, D'Lima D, Du J, Correlations of cortical bone microstructural and mechanical properties with water proton fractions obtained from ultrashort echo time (UTE) MRI tricomponent T2* model, NMR Biomed. 33 (2020) e4233. 10.1002/nbm.4233. [PubMed: 31820518]

[34]. Lu X, Jerban S, Wan L, Ma Y, Jang H, Le N, Yang W, Chang EYEY, Du J, Three Dimensional Ultrashort Echo Time Imaging with Tri-component Analysis for Human Cortical Bone, Magn Reson Med. 82 (2019) 348–355. 10.1002/mrm.27718. [PubMed: 30847989]

[35]. Hong AL, Ispiryan M, Padalkar M. v., Jones BC, Batzdorf AS, Shetye SS, Pleshko N, Rajapakse CS, MRI-derived bone porosity index correlates to bone composition and mechanical stiffness, Bone Rep. 11 (2019). 10.1016/j.bonr.2019.100213.

[36]. ASTM, Standard Test Methods for Flexural Properties of Unreinforced and Reinforced Plastics and Electrical Insulating Materials 1, Annual Book of ASTM Standards. (2011) 1–11. 10.1520/D0790-10.

[37]. Jerban S, Ma Y, Dorthe EW, Kakos L, Le N, Alenezi S, Sah RL, Chang EY, D'Lima D, Du J, Assessing cortical bone mechanical properties using collagen proton fraction from ultrashort echo time magnetization transfer (UTE-MT) MRI modeling, Bone Rep. 8 (2019) 1–8. 10.1016/j.bonr.2019.100220.

[38]. Koudelka P, Jiroušek O, Valach J, Determination of mechanical properties of materials with complex inner structure using microstructural models, Machines, Technologies, Materials. 1 (2011) 39–42.

[39]. Weibull W, A statistical Theory of the strength of materials, 1939.

[40]. Quinn JB, Quinn GD, A practical and systematic review of Weibull statistics for reporting strengths of dental materials, Dental Materials. 26 (2010) 135–147. 10.1016/j.dental.2009.09.006. [PubMed: 19945745]

[41]. Seifert AC, Li C, Wehrli SL, Wehrli FW, A Surrogate Measure of Cortical Bone Matrix Density by Long T2-Suppressed MRI, Journal of Bone and Mineral Research. 30 (2015) 2229–2238. 10.1002/jbmr.2580. [PubMed: 26085307]

[42]. Fernández-Seara MA, Wehrli SL, Takahashi M, Wehrli FW, Water Content Predicts Bone Mineral Density and Mechanical Properties, Journal Of Bone And Joint Surgery American Volume. 19 (2004) 289–295. 10.1359/JBMR.0301227.

[43]. Horch RA, Gochberg DF, Nyman JS, Does MD, Non-invasive predictors of human cortical bone mechanical properties: T2-Discriminated 1H NMR compared with high resolution X-ray, PLoS One. 6 (2011) 1–5. 10.1371/journal.pone.0016359.

[44]. Granke M, Makowski AJ, Uppuganti S, Does MD, Nyman JS, Identifying Novel Clinical Surrogates to Assess Human Bone Fracture Toughness, Journal of Bone and Mineral Research. 30 (2015) 1290–1300. 10.1002/jbmr.2452. [PubMed: 25639628]

[45]. Bae WC, Chen PC, Chung CB, Masuda K, D'Lima D, Du J, Quantitative ultrashort echo time (UTE) MRI of human cortical bone: Correlation with porosity and biomechanical properties, Journal of Bone and Mineral Research. 27 (2012) 848–857. 10.1002/jbmr.1535. [PubMed: 22190232]

[46]. Manhard MK, Uppuganti S, Granke M, Gochberg DF, Nyman JS, Does MD, MRI-derived bound and pore water concentrations as predictors of fracture resistance, Bone. 87 (2016) 1–10. 10.1016/j.bone.2016.03.007. [PubMed: 26993059]

[47]. Chang EY, Bae WC, Shao H, Biswas R, Li S, Chen J, Patil S, Healey R, Lima DDD, Chung CB, Du J, Ultrashort echo time magnetization transfer (UTE-MT) imaging of cortical bone, NMR Biomed. 28 (2015) 873–880. 10.1002/nbm.3316. [PubMed: 25981914]

[48]. Jerban S, Ma Y, Dorthe EW, Kakos L, Le N, Alenezi S, Sah RL, Chang EY, D'Lima D, Du J, Assessing cortical bone mechanical properties using collagen proton fraction from ultrashort echo time magnetization transfer (UTE-MT) MRI modeling, Bone Rep. 8 (2019). 10.1016/j.bonr.2019.100220.

[49]. Wan L, Zhao W, Ma Y, Jerban S, Searleman ACACAC, Carl M, Chang EYEY, Tang G, Du J, Fast quantitative 3D ultrashort echo time MRI of cortical bone using extended cones sampling, Magn Reson Med. 82 (2019) 225–236. 10.1002/mrm.27715. [PubMed: 30821032]

[50]. Lustig M, Donoho D, Pauly JM, Sparse MRI: The application of compressed sensing for rapid MR imaging, Magn Reson Med. 58 (2007) 1182–1195. 10.1002/mrm.21391. [PubMed: 17969013]

[51]. Athertya JS, Ma Y, Masoud Afsahi A, Lombardi AF, Moazamian D, Jerban S, Sedaghat S, Jang H, Accelerated Quantitative 3D UTE-Cones Imaging Using Compressed Sensing, Sensors. 22 (2022) 7459. 10.3390/s22197459. [PubMed: 36236557]

[52]. Otazo R, Kim D, Axel L, Sodickson DK, Combination of compressed sensing and parallel imaging for highly accelerated first-pass cardiac perfusion MRI, Magn Reson Med. 64 (2010) 767–776. 10.1002/mrm.22463. [PubMed: 20535813]

[53]. Chang G, Deniz CM, Honig S, Rajapakse CS, Egol K, Regatte RR, Brown R, Feasibility of three-dimensional MRI of proximal femur microarchitecture at 3 tesla using 26 receive elements without and with parallel imaging, Journal of Magnetic Resonance Imaging. 40 (2014) 229–238. 10.1002/jmri.24345. [PubMed: 24711013]

[54]. Ma Y-J, Jang H, Wei Z, Cai Z, Xue Y, Lee RR, Chang EY, Bydder GM, Corey-Bloom J, Du J, Myelin Imaging in Human Brain Using a Short Repetition Time Adiabatic Inversion Recovery Prepared Ultrashort Echo Time (STAIR-UTE) MRI Sequence in Multiple Sclerosis, Radiology. 297 (2020) 392–404. 10.1148/radiol.2020200425. [PubMed: 32779970]

[55]. Ma YJ, Chen Y, Li L, Cai Z, Wei Z, Jerban S, Jang H, Chang EYEY, Du J, Eric Y. Chang, Du J, Li L, Cai Z, Wei Z, Jerban S, Jang H, Chang EYEY, Du J, Trabecular bone imaging using a 3D adiabatic inversion recovery prepared ultrashort TE Cones sequence at 3T, Magn Reson Med. 83 (2020) 1640–1651. 10.1002/mrm.28027. [PubMed: 31631404]

[56]. Woessner DE, An NMR investigation into the range of the surface effect on the rotation of water molecules, Journal of Magnetic Resonance (1969). 39 (1980) 297–308. 10.1016/0022-2364(80)90138-9.

[57]. Du J, Takahashi AM, Bae WC, Chung CB, Bydder GM, Dual inversion recovery, ultrashort echo time (DIR UTE) imaging: Creating high contrast for short-T2species, Magn Reson Med. 63 (2010) 447–455. 10.1002/mrm.22257. [PubMed: 20099332]

[58]. Du J, Carl M, Bae WC, Statum S, Chang EY, Bydder GM, Chung CB, Dual inversion recovery ultrashort echo time (DIR-UTE) imaging and quantification of the zone of calcified cartilage (ZCC), Osteoarthritis Cartilage. 21 (2013) 77–85. 10.1016/j.joca.2012.09.009. [PubMed: 23025927]

[59]. Garwood M, DelaBarre L, The return of the frequency sweep: Designing adiabatic pulses for contemporary NMR, Journal of Magnetic Resonance. 153 (2001) 155–177. 10.1006/jmre.2001.2340. [PubMed: 11740891]

[60]. Ma YJ, Zhu Y, Lu X, Carl M, Chang EY, Du J, Short T 2 imaging using a 3D double adiabatic inversion recovery prepared ultrashort echo time cones (3D DIR-UTE-Cones) sequence, Magn Reson Med. 00 (2017) 1–9. 10.1002/mrm.26908.

[61]. Garwood M, DelaBarre L, The Return of the Frequency Sweep: Designing Adiabatic Pulses for Contemporary NMR, Journal of Magnetic Resonance. 153 (2001) 155–177. 10.1006/jmre.2001.2340. [PubMed: 11740891]

[62]. Wölfel EM, Fiedler IAK, Dragoun Kolibova S, Krug J, Lin M-C, Yazigi B, Siebels AK, Mushumba H, Wulff B, Ondruschka B, Püschel K, Glüer CC, Jähn-Rickert K, Busse B, Human tibial cortical bone with high porosity in type 2 diabetes mellitus is accompanied by distinctive bone material properties, Bone. 165 (2022) 116546. 10.1016/j.bone.2022.116546. [PubMed: 36113843]

[63]. Wölfel EM, Fiedler IAK, Dragoun Kolibova S, Krug J, Lin M-C, Yazigi B, Siebels AK, Mushumba H, Wulff B, Ondruschka B, Püschel K, Glüer CC, Jähn-Rickert K, Busse B, Human tibial cortical bone with high porosity in type 2 diabetes mellitus is accompanied by distinctive bone material properties, Bone. 165 (2022) 116546. 10.1016/j.bone.2022.116546. [PubMed: 36113843]

[64]. Farr JN, Drake MT, Amin S, Melton LJ, McCready LK, Khosla S, In Vivo Assessment of Bone Quality in Postmenopausal Women With Type 2 Diabetes, Journal of Bone and Mineral Research. 29 (2014) 787–795. 10.1002/jbmr.2106. [PubMed: 24123088]

[65]. Holloway-Kew KL, Betson A, Rufus-Membere PG, Gaston J, Diez-Perez A, Kotowicz MA, Pasco JA, Impact microindentation in men with impaired fasting glucose and type 2 diabetes, Bone. 142 (2021) 115685. 10.1016/j.bone.2020.115685. [PubMed: 33049369]
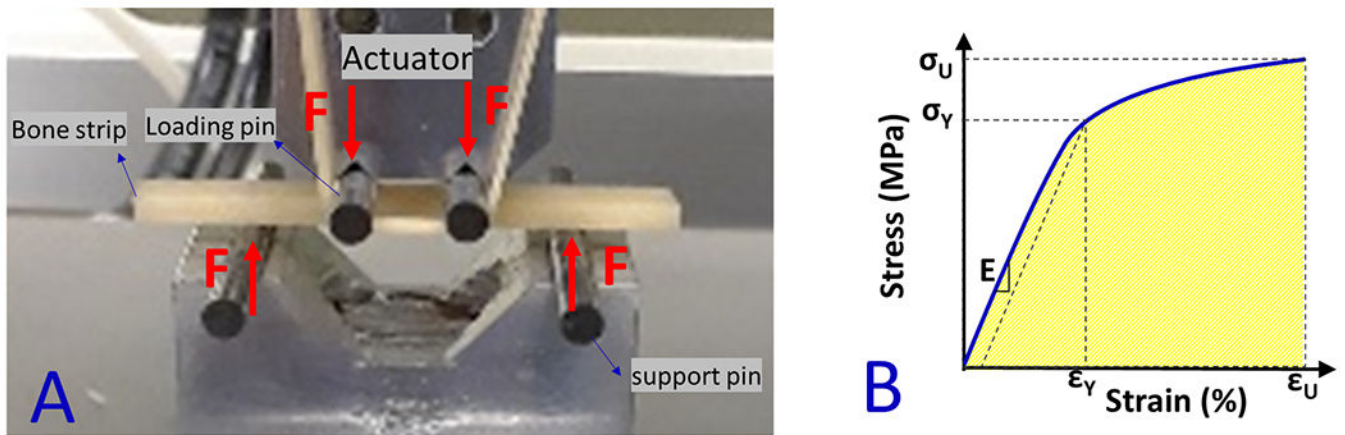
Figure 1:
(A) Prepared bone strips mounted on the fabricated four-point bending jigs (aluminum holders and tungsten carbide pins) mounted on an Instron 8511.20 machine. The experiments were displacement-controlled at 0.1 mm/s rates when the force was recorded. (B) Schematics stress-strain curve for calculating the mechanical properties such as Young's modulus (E), yield stress (σ_Y), yield strain (ε_Y), ultimate stress (σ_U), ultimate strain (ε_U), and failure energy (W_f).
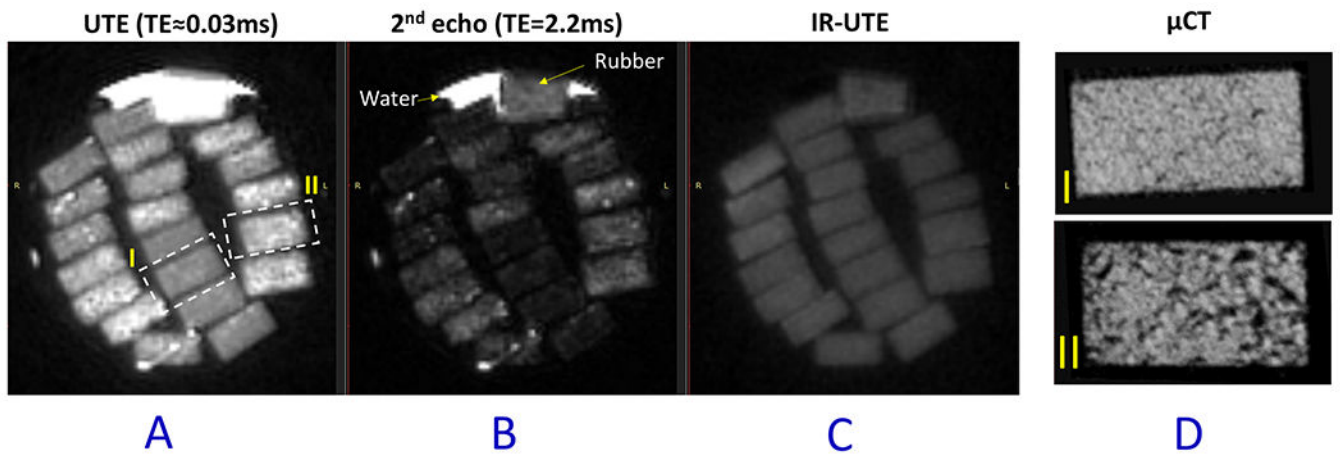
Figure 2:
(A) UTE-MRI (TE = 0.032 ms), (B) 2nd echo MRI image at TE = 2.2 ms, and (C) IR-UTE
(TE = 0.032 ms) images of twenty cortical bone strips with 4mm×2mm cross-sections.
(D) μCT images of two representative cortical bone strips from a 47-year-old male and a
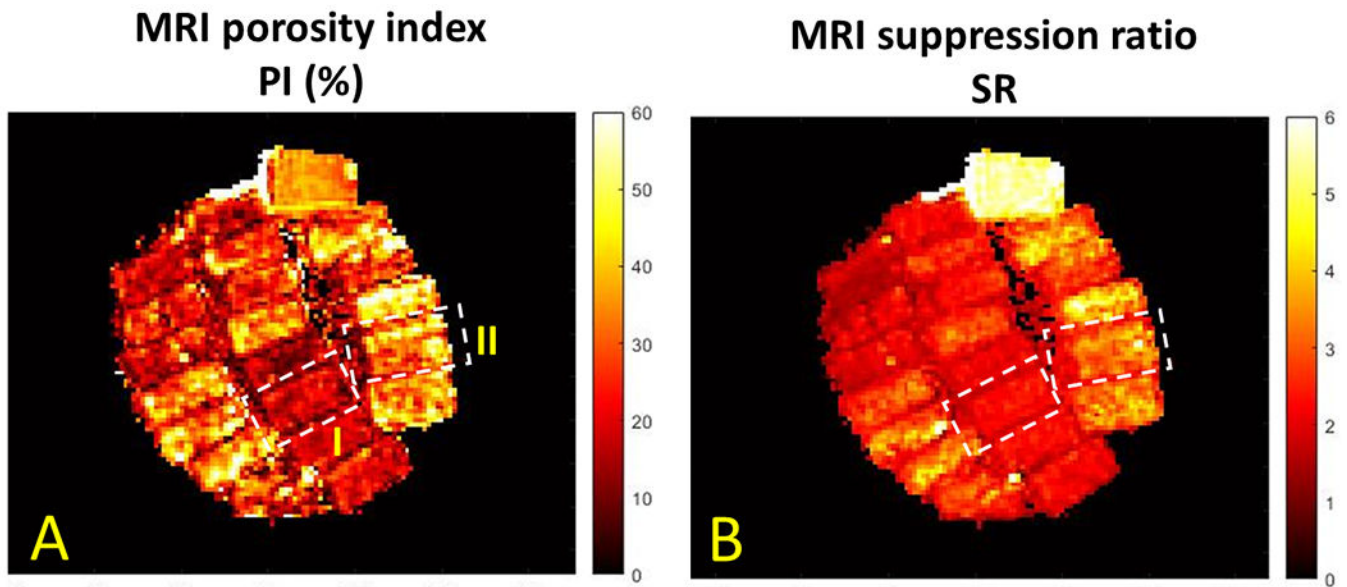57-year-old female, with 15% and 33% average porosities, respectively.

Figure 3:
(A) MRI-based porosity index (PI) and (B) suppression ratio (SR) pixel maps calculated for the twenty cortical bone strips shown in Figure 2. Specimen II (porosity of 33%, the lower sample in Figure 2D) demonstrates higher PI and SR values than specimen I (porosity of 15%, the upper sample in Figure 2D).
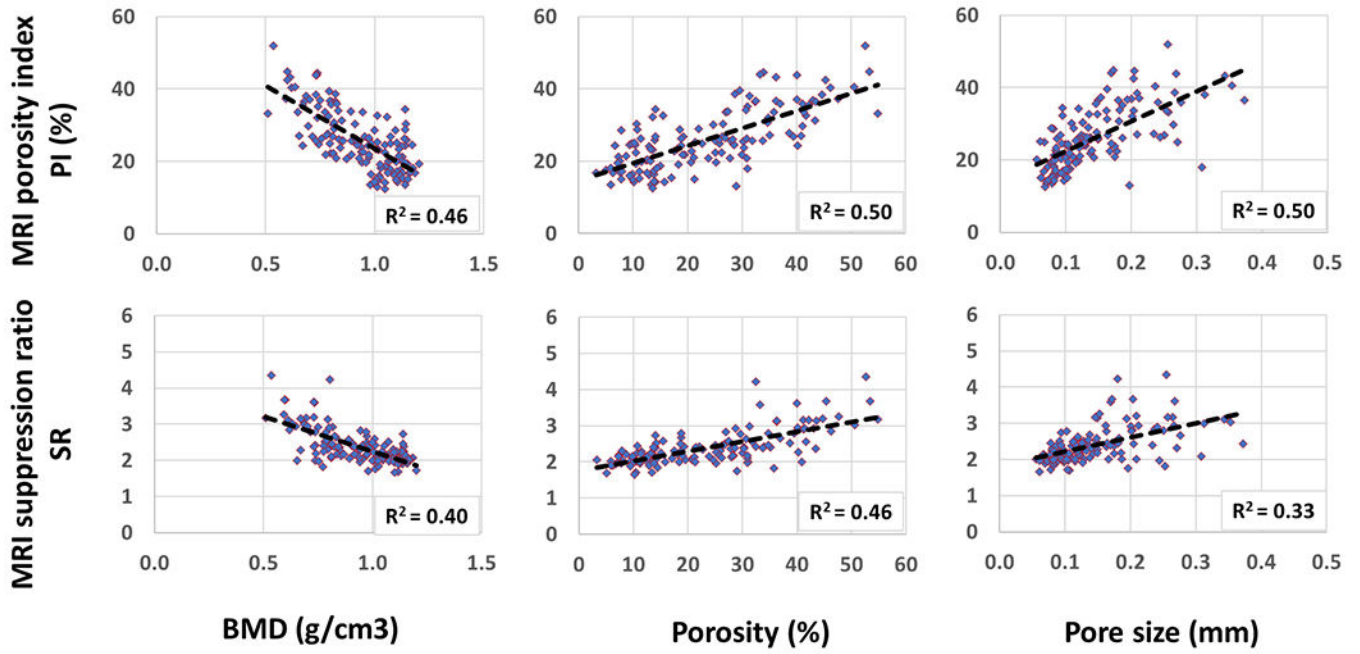
Figure 4:
Scatterplots and linear trendlines of PI and SR versus µCT-based BMD, porosity, and pore size. R^2 values were calculated from Spearman's correlation coefficients.
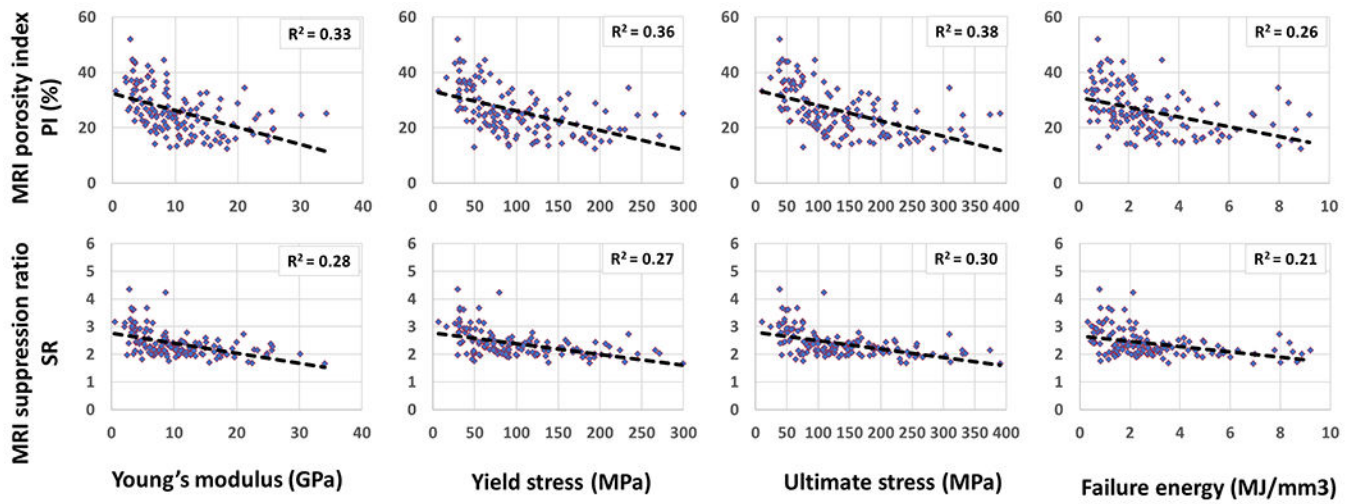
Figure 5:

Scatterplots and linear trendlines of PI and SR versus Young's modulus, yield stress, ultimate stress, and failure energy, respectively. R^2 values were calculated from Spearman's correlation coefficients.

Table 1:

The average, standard deviation (SD), and ranges of MRI, µCT, and mechanical properties of 135 bone strips.

PI (%)	SR (A.U.)	BMD (gr/cm3)	Porosity (%)	Pore size (mm)	Young's modulus (GPa)	Yield stress (MPa)	Ultimate stress (MPa)	Failure energy (MJ/mm3)
26.0±8.3 [12.5-52.0]	2.4±0.5 [1.7-4.3]	0.9±0.2 [0.5-1.2]	23.5±12.6 [3.2-54.9]	0.14±0.07 [0.06-0.37]	10.3±6.5 [0.5-34.1]	100.2±60.7 [6.7-299.4]	136.1±80.5 [10.1-390.9]	2.8±2.0 [0.3-9.2]

Table 2:

Spearman's correlation coefficients between MRI-based measures and microstructural and mechanical properties of cortical bone strips. All bone strips were considered as independent samples (n=135).

	PI	SR	BMD	Porosity	Pore size	Young's modulus	Yield stress	Ultimate stress	Failure energy
PI	1.00	0.79 (P<0.01)	−0.68 (P<0.01)	0.71 (P<0.01)	0.71 (P<0.01)	−0.57 (P<0.01)	−0.60 (P<0.01)	−0.62 (P<0.01)	−0.51 (P<0.01)
SR	0.79 (<P<0.01)	1.00	−0.63 (P<0.01)	0.68 (P<0.01)	0.58 (P<0.01)	−0.53 (P<0.01)	−0.52 (P<0.01)	−0.55 (P<0.01)	−0.46 (P<0.01)
BMD	−0.68 (P<0.01)	−0.63 (P<0.01)	1.00	−0.93 (P<0.01)	−0.76 (P<0.01)	0.76 (P<0.01)	0.80 (P<0.01)	0.81 (P<0.01)	0.61 (P<0.01)
Porosity	0.71 (<P<0.01)	0.68 (P<0.01)	−0.93 (P<0.01)	1.00	0.80 (P<0.01)	−0.76 (P<0.01)	−0.78 (P<0.01)	−0.79 (P<0.01)	−0.59 (P<0.01)
Pore size	0.71 (<P<0.01)	0.58 (P<0.01>)	−0.76 (P<0.01)	0.80 (P<0.01)	1.00	−0.72 (P<0.01)	−0.77 (P<0.01)	−0.79 (P<0.01)	−0.63 (P<0.01)